Chinese Physics Letters **42**, 061201 (2025) **Express Letter**

Vortex Mössbauer Effect as Nanoscale Probe of Chiral Structures

Yixin Li, Youjing Wang, Kai Zhao, Zhiguo Ma, Yumiao Wang,
Yi Yang, Xiangjin Kong, Changbo Fu*, and Yu-Gang Ma*

Key Lab of Nuclear Physics and Ion-beam Application (MoE), Institute of Modern Physics, Fudan University, Shanghai 200433, China

(Received 23 April 2025; accepted manuscript online 6 May 2025)

Chirality, a common phenomenon in nature, appears in structures ranging from galaxies and condensed matter to atomic nuclei. There is a persistent demand for new, high-precision methods to detect chiral structures, particularly at the microscale. Here, we propose a novel method, vortex Mössbauer spectroscopy, for probing chiral structures. By leveraging the orbital angular momentum carried by vortex beams, this approach achieves high precision in detecting chiral structures at scales ranging from nanometers to hundreds of nanometers. Our simulation shows the ratio of characteristic lines in the Mössbauer spectra of ^{57}Fe under vortex beams exhibits differences of up to four orders of magnitude for atomic structures with different arrangements. Additionally, simulations reveal the response of ^{229m}Th chiral structures to vortex beams with opposite angular momenta differs by approximately 49-fold. These significant spectral variations indicate that this new vortex Mössbauer probe holds great potential for investigating the microscopic chiral structures and interactions of matter.

DOI: 10.1088/0256-307X/42/6/061201 CSTR: 32039.14.0256-307X.42.6.061201

Introduction. Since the discovery of the Mössbauer effect[1] in 1958, Mössbauer spectroscopy[2] has become a powerful tool for studying the properties of materials at the atomic level, providing insights into material structures, including lattice structure,[3,4] chemical bonding,[5,6] phase transitions,[7,8] defects,[9] and magnetic properties.[10] Due to its versatility, this effect has found numerous applications in various scientific and technological areas, including physics, chemistry, biology, materials science, and archaeology.[11] The phenomenon represents a pivotal discovery in both nuclear and solid-state physics, revolutionizing our understanding of atomic processes and paving the way for numerous scientific and technological advancements. Conventional Mössbauer spectroscopy typically utilizes plane-wave beams. However, twisted (vortex) beams offer new opportunities, allowing for the probing of nanoscale chiral structures and their dynamic interactions with lattice or spin degrees of freedom.[12,13]

The concept of a vortex beam stems from the field of optics, where scientists explore novel ways to manipulate the properties of light.[14–19] In 1992, researcher Allen[20] proposed the idea of using helical phase structures in light beams to encode additional information. It was understood that, similar to physical objects possessing orbital angular momentum (OAM), light beams could also carry OAM due to their helical phase structure.[21–23] This distinctive property allows vortex laser beams to carry additional information and perform various tasks, making them valuable in diverse applications such as optical tweezers for manipulating microparticles,[24] quantum information processing,[25] imaging,[26–28] and material processing. Today, vortex laser beams remain an active area of research,[29–31] with ongoing efforts focused on refining their properties, exploring new applications, and integrating them into practical technologies.[32–38]

Different materials display unique structures due to diverse atomic arrangements and interactions. Among them is the chiral structure, which ubiquitously exists in entities such as galaxies, fluids, protein molecules, Bose-Einstein condensates (BECs), Rayleigh-Bénard convection cells, Abrikosov flux lattices,[12,39,40] and so on. The behavior and dynamics of chiral interactions are of great theoretical and experimental interest.[41–46] These chiral structures play a crucial role in determining the macroscopic properties and behaviors of the materials in which they exist. To study chiral structures, especially in condensed matter physics, dedicated probes are essential. Existing probes capable of detecting microscopic chiral structures, such as scanning electron microscopy (SEM),[47] are limited to detecting surface vortices in condensed matter. Probes capable of penetrating deeper into internal structures are needed.

In this paper, we present a novel method for investigating chiral structures by utilizing the Mössbauer effect with vortex beams. Firstly, we develop the theory of Mössbauer spectroscopy under a vortex beam, which exhibits distinct characteristics compared with that under a plane wave. Secondly, taking ^{57}Fe and ^{229m}Th as examples, we analyze the models of chiral targets in detail. It is demonstrated that the Mössbauer spectroscopy under vortex beams with chiral properties can serve as a powerful probe for investigating chiral structures in condensed matter.

Vortex Mössbauer Theory. For a Bessel vortex beam

*Corresponding author. Email: cbfu@fudan.edu.cn; mayugang@fudan.edu.cn
© 2025 Chinese Physical Society and IOP Publishing Ltd. All rights, including for text and data mining, AI training, and similar technologies, are reserved.

propagating along the z-axis, with total momentum $\boldsymbol{k}$ and transverse momentum $\boldsymbol{k}_\perp$, the vector potential can be written as [48]

$$\boldsymbol{A}^{(\mathrm{vor})}_{\kappa m_\gamma k_z \lambda}(\boldsymbol{r},t)=\int \boldsymbol{e}_{\boldsymbol{k}\lambda}\mathrm{e}^{\mathrm{i}\boldsymbol{k}\cdot\boldsymbol{r}}\mathrm{e}^{-\mathrm{i}\omega t}a_{\kappa m_\gamma}(\boldsymbol{k}_\perp)\frac{\mathrm{d}^2\boldsymbol{k}_\perp}{(2\pi)^2}, \quad (1)$$

where $\lambda=\pm1$ is the photon helicity; l_γ is the vortex beam's orbital angular momentum (OAM) quantum number; [49] $m_\mathrm{s}=0,\pm\lambda$ represents the spin angular momentum projection; $m_\gamma=l_\gamma+m_\mathrm{s}$ is the total angular momentum (TAM) projected onto the z-axis.

As detailed in the Supplementary Material (SM), when the vortex photon beam is scattered by a nucleus located at an off-axis position $\boldsymbol{b}$ [Fig. 1(a)], the scattering cross section can be written as

$$\sigma^{(\mathrm{vor})}_{m_\mathrm{i}m_\mathrm{f}}(\theta_{\boldsymbol{k}},\boldsymbol{b},m_\gamma)\triangleq\frac{\pi^2a^2\delta(\Delta E)}{k\cos\theta_{\boldsymbol{k}}\,j}|J_{m_\gamma+m_\mathrm{i}-m_\mathrm{f}}(\kappa b)|^2 \cdot\left|\sum_{m_\mathrm{i}'m_\mathrm{f}'}\mathrm{d}^{J_\mathrm{i}}_{m_\mathrm{i}m_\mathrm{i}'}(\theta_{\boldsymbol{k}})\mathrm{d}^{J_\mathrm{f}}_{m_\mathrm{f}m_\mathrm{f}'}(\theta_{\boldsymbol{k}})M^{(\mathrm{pl})}_{m_\mathrm{i}'m_\mathrm{f}'}\right|^2, \quad (2)$$

where m_f, $m_\mathrm{f}'\in[-J_\mathrm{f},J_\mathrm{f}]$; m_i, $m_\mathrm{i}'\in[-J_\mathrm{i},J_\mathrm{i}]$; $\mathrm{d}^j_{mm'}(\theta)=\langle jm'|\mathrm{e}^{-\mathrm{i}\theta j_y/\hbar}|jm\rangle$ is the Wigner's d-matrix; and $M^{(\mathrm{pl})}_{m_1m_2}$ is the transition matrix of plane wave.

Taking ^{57}Fe as an example, when $m_\gamma=2$ and $\lambda=1$, the Mössbauer absorption cross section $\sigma^{(\mathrm{vor})\mathrm{Fe}}_{m_\mathrm{i}m_\mathrm{f}}(\theta_{\boldsymbol{k}},\boldsymbol{b},m_\gamma)$ between the ground state ($J_\mathrm{i}=\frac{1}{2}$) and the excited state ($J_\mathrm{f}=\frac{3}{2}$), as shown in Fig. 1(b), can be calculated using the Eq. (2) and Table SI in the SM. It can be observed that although conservation of angular momentum still holds, the traditional selection rule $\Delta m=\lambda$, derived from the plane wave, no longer holds. This is due to the fact that the vortex photon beams carry nonzero OAM and spin angular momentum (SAM) at the same time. [49] See the SM for more details.

If more than one nucleus are serving as target, Eq. (2) should be modified. If the scattering from all the nuclei in the target is incoherent, the average scattering cross section of a Bessel vortex beam [50] can be written as

$$\bar{\sigma}^{(\mathrm{vor,inc})}_{m_\mathrm{i}m_\mathrm{f}}(\theta_{\boldsymbol{k}},m_\gamma)\propto\int_0^R J^2_{m_\gamma-\Delta m}(\kappa b)|M^{(\mathrm{pl})}_{m_\mathrm{i}m_\mathrm{f}}(\theta_{\boldsymbol{k}})|^2\mathrm{d}\boldsymbol{b}, \quad (3)$$

where R is the radius of the Bessel beam.

Following Eq. (S28) in the SM, the photon absorption number is calculated to get Fig. 2, which shows the dependence of the relative scale $\Delta N^{(\mathrm{vor})}_{m_\mathrm{i}m_\mathrm{f}}(\theta_{\boldsymbol{k}},m_\gamma)/\sum_{m_\mathrm{i}m_\mathrm{f}}\Delta N^{(\mathrm{vor})}_{m_\mathrm{i}m_\mathrm{f}}(\theta_{\boldsymbol{k}},m_\gamma)$ of line transitions on $\theta_{\boldsymbol{k}}$ angles, where $\theta_{\boldsymbol{k}}\in[0,\pi/2]$. At $\theta_{\boldsymbol{k}}=0$, only two transition spectral lines are discernible. With the increase of $\theta_{\boldsymbol{k}}$, the distinctive characteristics of vortex beams become progressively more pronounced. Consequently, the proportion of the other four transition spectral lines gradually increases, surpassing the constraints of traditional nuclear selection rules. An interesting finding is that by adjusting $\theta_{\boldsymbol{k}}$, one can enhance the specific spectral line they wish to detect. For example, when $\theta_{\boldsymbol{k}}=60^\circ$, the number of photons absorbed by the $\frac{1}{2}\to\frac{1}{2}$ transition is more than that of the $-\frac{1}{2}\to\frac{1}{2}$ transition, reaching about $\Delta N_{\frac{1}{2}\frac{1}{2}}(\theta_{\boldsymbol{k}}=60^\circ,m_\gamma=2)/\sum_{m_\mathrm{i}m_\mathrm{f}}\Delta N(\theta_{\boldsymbol{k}}=60^\circ,m_\gamma=2)=0.25$, which can be observed easily in experiments. When $\theta_{\boldsymbol{k}}=0$, as expected, the vortex wave returns to the plane wave and then, as an example, $\Delta N_{-\frac{1}{2}\frac{1}{2}}(\theta_{\boldsymbol{k}}=0^\circ,m_\gamma=2):\Delta N_{\frac{1}{2}\frac{3}{2}}(\theta_{\boldsymbol{k}}=0^\circ,m_\gamma=2)=1:3$, which is the same as that in the plane wave case. [2]

However, the coherence length of a Bessel beam can be much larger than the size of the target, and then the cross section should be

$$\bar{\sigma}^{(\mathrm{vor,coh})}_{m_\mathrm{i}m_\mathrm{f}}\propto\left|\int_0^R\mathrm{e}^{\mathrm{i}(m_\gamma-\Delta m)\varphi_b}J_{m_\gamma-\Delta m}(\kappa b)M^{(\mathrm{pl})}_{m_\mathrm{i}m_\mathrm{f}}(\theta_{\boldsymbol{k}})\mathrm{d}\boldsymbol{b}\right|^2. \quad (4)$$

This equation shows that vortex beams, with their unique degree of freedom in OAM and long coherence length, allow for extracting much more detailed information about the chiral structure of targets (the phase of the wave function $\mathrm{e}^{\mathrm{i}(m_\gamma-\Delta m)\varphi_b}$) by taking Mössbauer spectra [51] with vortex beams, as compared to plane waves.

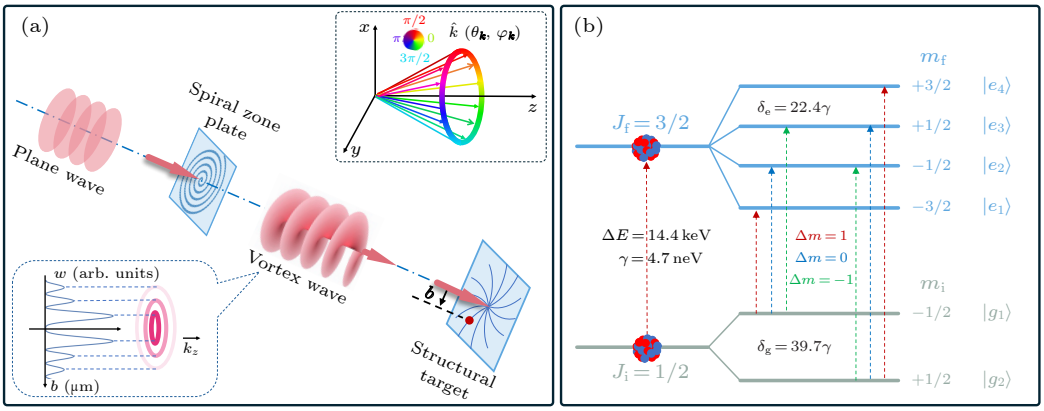

Fig. 1. (a) A plane wave incident on a spiral zone plate with topological charges generates the vortex wave. Top-right inserted: the wave vectors $\boldsymbol{k}$ distribute on a conical surface with a polar angle $\theta_{\boldsymbol{k}}=\arctan(|\boldsymbol{k}_\perp|/k_z)$. Bottom-left inserted: the density distribution of a Bessel beam with $m_\gamma=2$, with a hole in the center. (b) A diagram illustrating possible Mössbauer transition lines of ^{57}Fe under a plane wave or vortex wave. The ground state $J_\mathrm{i}=1/2$ splits into two levels $m_\mathrm{i}=\pm1/2$; and the excited state $J_\mathrm{f}=3/2$ splits into four levels $m_\mathrm{f}=\pm3/2$, $\pm1/2$. According to the traditional selection rules, the plane wave beam with $\lambda=1$ can only trigger the transitions of $\Delta m=\lambda$; while for the vortex beam with $\lambda=1$ and $m_\gamma=2$, the traditional selection rules, $\Delta m=\lambda$ is broken.

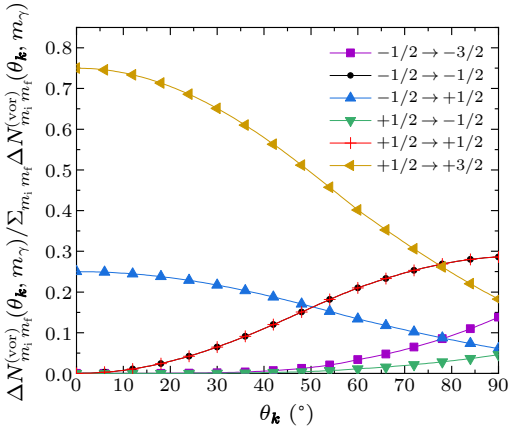

Fig. 2. The relative ratio $\Delta N^{(\mathrm{vor})}_{m_i m_f}(\theta_{\boldsymbol{k}}, m_\gamma)/[\sum_{m_i' m_f'} \Delta N^{(\mathrm{vor})}_{m_i' m_f'}(\theta_{\boldsymbol{k}}, m_\gamma)]$ calculated by Eqs. (3) and (S24) in the SM, as a function of the polar angle $\theta_{\boldsymbol{k}}$ for different transition lines. Here, take $m_\gamma = 2$ and $\lambda = 1$.

^{57}Fe *Chiral Probe.* With advancements in technologies like high-order harmonic generation (HHG), the feasibility of producing short-wavelength vortex beams has significantly increased,[52–54] enabling the expected generation of vortex photons in the ultraviolet to soft X-ray range by modulating high-order harmonics. Furthermore, leveraging free-electron laser (FEL) technology, vortex photon energies can be further enhanced to X-ray wavelengths.[55–57] For example, recent papers have reported X-rays with orbital angular momentum (OAM) at keV energies and nanometer-scale wavelengths.[58] Therefore, studying the Mössbauer effect of ^{57}Fe using X-ray vortex beams with an energy of 14.4 keV in laboratories is possible in the future.

As an example, simplified models for both beams and targets are taken (Fig. 3). The incident beams are modeled as an array of vortex beams periodically arranged in space, and the structural targets are arranged into different configurations on a two-dimensional plane, as shown in Figs. 3(a) and 3(b), where (a) is a periodic hexagon and (b) is a quadrilateral.

When performing the numerical simulation, a two-dimensional chiral distribution array is generated [Fig. 3(a) insert], and the absorbed photon number $\Delta N^{(\mathrm{vor})}_{m_i m_f}(\theta_{\boldsymbol{k}}, m_\gamma)$ is expressed as Eq. (S30) in the SM. The centers of the chiral distribution are located at the center of the atomic equilibrium position.

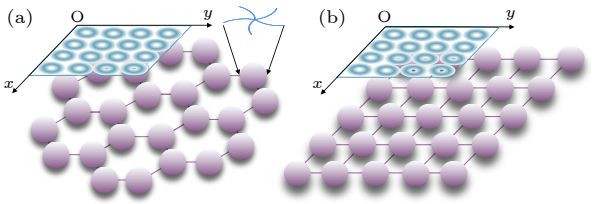

Fig. 3. Two tentative target structures for vortex Mössbauer. The incident vortex beam array acts on the two-dimensional structure, which is arranged in hexagonal and quadrilateral patterns. The relative position of each atomic nucleus at the atomic scale is modeled as a series of points following a two-dimensional chiral distribution, which models the effect of the chemical environment.[59]

We consider incident vortex beams with an energy of 14.4 keV, a polar angle $\theta_{\boldsymbol{k}} = 30°$ and $m_\gamma = 2$, as shown in Fig. 3(a). The calculation results of $r^{(\mathrm{vor})}_{m_i m_f}(m_\gamma)$, defined as

$$r^{(\mathrm{vor})}_{m_i m_f}(\theta_{\boldsymbol{k}}, m_\gamma) = \frac{\Delta N^{(\mathrm{vor})}_{m_i m_f}(\theta_{\boldsymbol{k}}, m_\gamma)}{\Delta N^{(\mathrm{vor})}_{\frac{1}{2}\frac{1}{2}}(\theta_{\boldsymbol{k}}, m_\gamma)}, \tag{5}$$

normalized to the photon count of the $\frac{1}{2} \to \frac{1}{2}$ transition, are given in Fig. 4. It can be observed that for both hexagonal and quadrilateral configurations, the vortex parameter m_γ significantly influences the transitional characteristic ratio $r^{(\mathrm{vor})}_{\frac{1}{2}\frac{3}{2}}(\theta_{\boldsymbol{k}}, m_\gamma)$, in contrast to the fixed ratio of 3:2 observed under plane wave incidence. For instance, when $m_\gamma = 0$ or 1, the absorption spectra of vortex beams for the two target structures differ by over four orders of magnitude.

Moreover, hexagonal and quadrilateral arrangements display significantly different $r^{(\mathrm{vor})}_{\frac{1}{2}\frac{3}{2}}(\theta_{\boldsymbol{k}}, m_\gamma)$ values under the same m_γ, as shown in Fig. 4. This further highlights the potential of vortex light as a powerful spectral tool for evaluating material structures.

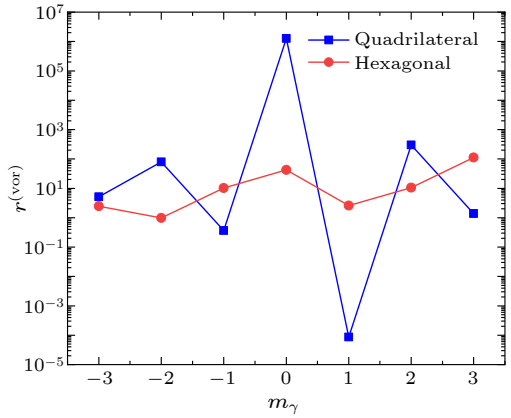

Fig. 4. The ratio $r^{(\mathrm{vor})}_{\frac{1}{2}\frac{3}{2}}(\theta_{\boldsymbol{k}}, m_\gamma)$ defined by Eq. (5) for the hexagonal and quadrilateral structure shown in Fig. 3, where $\theta_{\boldsymbol{k}} = 30°$, $m_\gamma = 2$ and $\lambda = 1$.

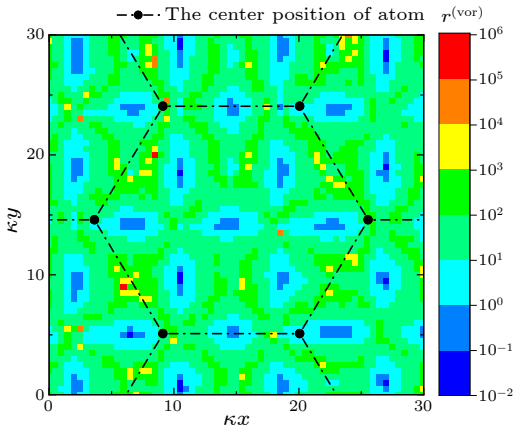

Fig. 5. Two-dimensional distribution of $r^{(\mathrm{vor})}_{\frac{1}{2}\frac{3}{2}}(\theta_{\boldsymbol{k}}, m_\gamma)$ when moving the relative position of the beam array and the target array along the x-y plane. Here we take the polar angle as $\theta_{\boldsymbol{k}} = 30°$, $m_\gamma = 2$, $\lambda = 1$, and $\kappa x \in [0, 30]$ and $\kappa y \in [0, 30]$.

By moving the relative position between the vortex beam array and the target array along the x and y directions, one can obtain two-dimensional spectra $r^{(\mathrm{vor})}_{m_\mathrm{i}m_\mathrm{f}}(\theta_{\boldsymbol{k}}, m_\gamma)$ as functions of x and y. The result is shown in Fig. 5. From an experimental perspective, once this type of pattern is obtained, the structure of the target can be deduced from it.[60]

$^{229\mathrm{m}}$Th *Chiral Probe.* Given the fact that the isomeric state $^{229\mathrm{m}}$Th, which has attracted widespread attention,[61–64] has an energy of about 8.4 eV,[65,66] corresponding to the wavelength of about 148 nm,[67,68] it holds great potential for further research in nuclear physics. It turns out that preparing vortex beams with a large polar angle is more feasible than generating ones with an energy of 14.4 keV, as in ^{57}Fe. With the rapid development of experimental technology, the Mössbauer resonance absorption spectrum of the $^{229\mathrm{m}}$Th nuclide has the potential to be realized.[65,69]

A tentative chiral structure, shown in Fig. 6, is employed in the subsequent simulations. A polar angle of $\theta_{\boldsymbol{k}} = 30^\circ$ is adopted, and the radial distance from the center of the vortex beam to the first intensity minimum of the beam is approximately $b = 200$ nm, which matches the characteristic scale of typical structures like BECs or Abrikosov flux lattices.[12,70] With modern technologies,

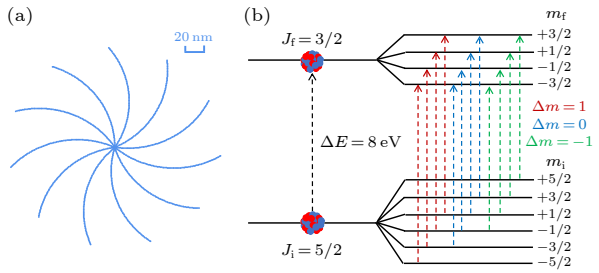

Fig. 6. (a) A tentative chiral structure; (b) The transition of $^{229\mathrm{m}}$Th between the ground ($J_\mathrm{i} = 5/2$) and the excited ($J_\mathrm{f} = 3/2$) states. In the presence of a magnetic hyperfine field, the ground state $J_\mathrm{i} = 5/2$ splits into six levels, $m_\mathrm{i} = \pm 5/2, \pm 3/2, \pm 1/2$, while the excited state $J_\mathrm{f} = 3/2$ splits into four levels, $m_\mathrm{f} = \pm 3/2, \pm 1/2$.

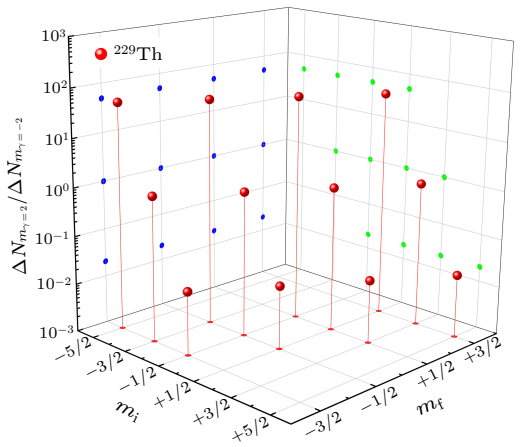

Fig. 7. The relative ratio, $\Delta N^{(\mathrm{vor})}_{m_\mathrm{i}m_\mathrm{f}}(m_\gamma = 2)/\Delta N^{(\mathrm{vor})}_{m_\mathrm{i}m_\mathrm{f}}(m_\gamma = -2)$, where $\Delta N^{(\mathrm{vor})}_{m_\mathrm{i}m_\mathrm{f}}$ is the number of photons absorbed by $^{229\mathrm{m}}$Th target when it is irradiated with a vortex beam. Here, $\theta_{\boldsymbol{k}} = 30^\circ$ and $\lambda = 1$ are used.

the coherence length of the incident beam, $\Delta\lambda$, can be much larger than the vortex beam radius, which is currently considered to be around a few μm. Therefore, the coherent scattering of the beam and the target must be taken into account.

The Mössbauer spectrum of $^{229\mathrm{m}}$Th has 12 transition lines,[71] as illustrated in Fig. 6. The transition probabilities for the various pathways are calculated using Eq. (4), and the corresponding $R^{\mathrm{Th}}_{m_\mathrm{i}m_\mathrm{f}}(\theta_{\boldsymbol{k}}) = |M^{(\mathrm{pl})}_{m_\mathrm{i}m_\mathrm{f}}(\theta_{\boldsymbol{k}})|^2/|M^{(\mathrm{pl})}_{-\frac{1}{2}\frac{1}{2}}|^2$ are presented in Table SII (see SM).

Using Eqs. (S24), (S25), and (S29) from the SM, and by taking $\theta_{\boldsymbol{k}} = 30^\circ$, $\lambda = 1$, and $m_\gamma = \pm 2$, the absorption ratios for different transition pathways are obtained and shown in Fig. 7.

Figure 7 shows that there is an order of magnitude difference in the ratio of absorbed photons in certain reaction channels when a material with a specific chiral structure interacts with vortex beams of opposite m_γ. For example, the absorption ratio for the $\frac{1}{2} \to \frac{3}{2}$ transition between $m_\gamma = +2$ and $m_\gamma = -2$ is given by $\Delta N^{(\mathrm{vor})}_{\frac{1}{2}\frac{3}{2}}(m_\gamma = 2)/\Delta N^{(\mathrm{vor})}_{\frac{1}{2}\frac{3}{2}}(m_\gamma = -2) \simeq 49$, which indicates that chiral targets have significantly different responses to vortex beams with opposite m_γ. Therefore, when vortex beams are used as a Mössbauer spectroscopic probe, such ratios can serve as characteristic observables for identifying the chiral properties of materials.

Summary. In this work, the Mössbauer effect under vortex beams has been investigated. Due to the topological charge carried by the vortex beams, the selection rules for plane waves are broken. Some transitions, which are forbidden for the plane wave case, become possible, and the strengths of the corresponding spectral lines is then adjusted according to the polar angle $\theta_{\boldsymbol{k}}$. This effect suggests that vortex beams can be used as an efficient probe for detecting chiral structures in condensed matter systems. After developing the general theory of the vortex Mössbauer effect, we apply the theory to two representative nuclei: ^{57}Fe and $^{229\mathrm{m}}$Th. The calculations show that the ratio between different absorption lines can serve as an indicator of the structural properties of the target materials, including chiral distributions, lattice structures, and other features. These results suggest that the new probe, the vortex Mössbauer effect, may open up an entirely new way to study the structure of unique materials. This probe could be used in the study of the microstructure of condensed matter physics, superconducting physics, nuclear physics, and more.

Acknowledgements. This work was supported in part by the National Key R&D Program (Grant No. 2023YFA1606900) and the National Natural Science Foundation of China (Grant No. 12235003).

References

[1] Principi G 2020 *Metals* **10** 992

[2] Greenwood N N and Gibb T C 2012 *Mössbauer spectroscopy* (Berlin: Springer Science Business Media)

[3] Błachowski A, Ruebenbauer K, Żukrowski J, and Bukowski Z 2014 *J. Alloys. Compd.* **582** 167
[4] Moreno M S and Mercader R C 1994 *Phys. Rev. B* **50** 9875
[5] Duncan J F and Golding R M 1965 *Q. Rev., Chem. Soc.* **19** 36
[6] Bancroft G M and Piatt R H 1972 *Mössbauer spectra of inorganic compounds: Bonding and structure* (Amsterdam: Elsevier) p. 59
[7] McGuire M A, Christianson A D, Sefat A S *et al.* 2008 *Phys. Rev. B* **78** 094517
[8] Beurmann P S, Thangadurai V, and Weppner W 2003 *J. Solid State Chem.* **174** 392
[9] Weyer G 2007 *Hyperfine Interact.* **77** 1
[10] Pohjonen R, Mustonen O, Karppinen M, and Lindén J 2018 *J. Alloys Compd.* **746** 135
[11] Wagner F E and Kyek A 2004 *Hyperfine Interact.* **154** 5
[12] Hess H F, Robinson R B, Dynes R C, Valles Jr J M, and Waszczak J V 1989 *Phys. Rev. Lett.* **62** 214
[13] Green D and Forbes K A 2023 *Nanoscale* **15** 540
[14] Shen Y J, Wang X J, Xie Z W, Min C J, Fu X, Liu Q, Gong M L, and Yuan X C 2019 *Light Sci. Appl.* **8** 90
[15] Padgett M, Courtial J, and Allen L 2004 *Phys. Today* **57** 35
[16] Shen Y J, Wan Z S, Meng Y, Fu X, and Gong M L 2018 *IEEE Photonics J.* **10** 1
[17] Saad F and Belafhal A 2023 *Opt. Quantum Electron.* **55** 83
[18] Saad F, El Halba E M, and Belafhal A 2016 *Opt. Quantum Electron.* **48** 1
[19] Hernández-García C, Vieira J, Mendonça J T, Rego L, San Román J, Plaja L, Ribic P R, Gauthier D, and Picón A 2017 *Photonics* **4** 28
[20] Allen L, Beijersbergen M W, Spreeuw R J C, and Woerdman J P 1992 *Phys. Rev. A* **45** 8185
[21] Gauthier D, Ribič P R, Adhikary G, Camper A, Chappuis C, Cucini R, DiMauro L F, Dovillaire G, Frassetto F, Géneaux R, Miotti P, Poletto L, Ressel B, Spezzani C, Stupar M, Ruchon T, and De Ninno G 2017 *Nat. Commun.* **8** 14971
[22] Lu Z W, Guo L, Ababekri M, Zhang J L, Weng X F, Wu Y B, Niu Y F, and Li J X 2025 *Phys. Rev. Lett.* **134** 052501
[23] Afanasev A, Carlson C E, Schmiegelow C T, Schulz J, Schmidt-Kaler F, and Solyanik M 2018 *New J. Phys.* **20** 023032
[24] Zhu L, Guo Z, Xu Q, Zhang J R, Zhang A J, Wang W, Liu Y, Wang X S, and Qu S L 2015 *Opt. Commun.* **354** 34
[25] Li Z X, Ruan Y P, Chen P, Tang J, Hu W, Xia K Y, and Lu Y Q 2021 *Chin. Opt. Lett.* **19** 112601
[26] Liu K, Cheng Y Q, Li X, Qin Y L, Wang H Q, and Jiang Y W 2016 *IEEE Antennas Wireless Propag. Lett.* **15** 1873
[27] Liu K, Cheng Y Q, Yang Z C, Wang H Q, Qin Y L, and Li X 2014 *IEEE Antennas Wireless Propag. Lett.* **14** 711
[28] Béché A, Juchtmans R, and Verbeeck J 2017 *Ultramicroscopy* **178** 12
[29] Kazinski P O and Ryakin V A 2021 *Russ. Phys. J.* **64** 717
[30] Kazinski P O and Ryakin V A 2023 *Ann. Phys.* **455** 169365
[31] Bogdanov O V, Kazinski P O, and Lazarenko G Y 2020 *JINST* **15** C04052
[32] Wu Y B, Gargiulo S, Carbone F, Keitel C H, and Pálffy A 2022 *Phys. Rev. Lett.* **128** 162501
[33] Pavlov I, Chaikovskaia A, and Karlovets D 2025 *Phys. Rev. C* **111** 024619
[34] Maiorova A V, Karlovets D, Fritzsche S, Surzhykov A, and Stöhlker T 2024 *New J. Phys.* **26** 093010
[35] Kazinski P O, Korolev P S, Lazarenko G Y, and Ryakin V A 2024 *Ann. Phys.* **462** 169610
[36] Karlovets D V 2012 *Phys. Rev. A* **86** 062102
[37] Ivanov I P and Karlovets D V 2013 *Phys. Rev. A* **88** 043840
[38] Maiorova A V, Peshkov A A, and Surzhykov A 2021 *Phys. Rev. A* **104** 022821
[39] Aftalion A 2007 *Vortices in Bose-Einstein Condensates* (Berlin: Springer Science and Business Media)
[40] Bergé P and Dubois M 1984 *Contemp. Phys.* **25** 535
[41] Campbell L J, Doria M M, and Kogan V G 1988 *Phys. Rev. B* **38** 2439
[42] Gilat G 1991 *Mol. Eng.* **1** 161
[43] Tverdislov V A, Malyshko E V, Il'chenko S A, Zhulyabina O A, and Yakovenko L V 2017 *Biophysics* **62** 331
[44] Wen Y, He M Q, Yu Y L, and Wang J H 2021 *Adv. Colloid Interface Sci.* **289** 102376
[45] Quack M 1989 *Angew. Chem. Int. Ed.* **28** 571
[46] Fedotov V A, Mladyonov P L, Prosvirnin S L, Rogacheva A V, Chen Y, and Zheludev N I 2006 *Phys. Rev. Lett.* **97** 167401
[47] Vinnikov L Y, Gurevich L A, Yemelchenko G A, and Ossipyan Y A 1988 *Solid State Commun.* **67** 421
[48] Ivanov I P 2022 *Prog. Part. Nucl. Phys.* **127** 103987
[49] Lu Z W, Guo L, Li Z Z, Ababekri M, Chen F Q, Fu C B, Lv C, Xu R R, Kong X J, Niu Y F, and Li J X 2023 *Phys. Rev. Lett.* **131** 202502
[50] Solyanik-Gorgone M 2019 *Interaction of Quantum Vortex Beams with Matter* (Ph.D. Dissertation) (Washington: The George Washington University)
[51] Gruverman I 2013 *Mössbauer effect methodology* (Berlin: Springer Science and Business Media)
[52] Gariepy G, Leach J, Kim K T, Hammond T J, Frumker E, Boyd R W, and Corkum Paul B 2014 *Phys. Rev. Lett.* **113** 153901
[53] Géneaux R, Camper A, Auguste T, Gobert O, Caillat J, Taïeb R, and Ruchon T 2016 *Nat. Commun.* **7** 12583
[54] Zürch M, Kern C, Hansinger P, Dreischuh A, and Spielmann C 2012 *Nat. Phys.* **8** 743
[55] Hemsing E, Knyazik A, O'Shea F, Marinelli A, Musumeci P, Williams O, Tochitsky S, and Rosenzweig J B 2012 *Appl. Phys. Lett.* **100** 091110
[56] Hemsing E, Musumeci P, Reiche S, Tikhoplav R, Marinelli A, Rosenzweig J B, and Gover A 2009 *Phys. Rev. Lett.* **102** 174801
[57] Hemsing E, Marinelli A, and Rosenzweig J B 2011 *Phys. Rev. Lett.* **106** 164803
[58] Geng H P 2020 *Exploration of X-ray correlation with orbital angular momentum based on accelerators* (Ph. D. Dissertation) (Shanghai: University of Chinese Academy of Sciences)
[59] Zhao G Q and Ren Z G 1989 *Nuclear analysis technique* (Beijing: Atomic energy Press)
[60] Goodman J W 2005 *Introduction to Fourier optics* (Greenwood Village: Roberts and Company publishers)
[61] Zhao J Y, Pálffy A, Keitel C H, and Wu Y B 2024 *Phys. Rev. C* **110** 014330
[62] Kirschbaum T, Minkov N, and Pálffy A 2024 *Phys. Rev. C* **105** 064313
[63] Nickerson B S, Pimon M, Bilous P V, Gugler J, Beeks K, Sikorsky T, Mohn P, Schumm T, and Pálffy A 2020 *Phys. Rev. Lett.* **125** 032501
[64] Müller R A, Maiorova A V, Fritzsche S, Volotka A V, Beerwerth R, Glowacki P, Thielking J, Meier D M, Okhapkin M, Peik E, and Surzhykov A 2018 *Phys. Rev. A* **98** 020503
[65] Tiedau J, Okhapkin M V, Zhang K, Thielking J, Zitzer G, Peik E, Schaden F, Pronebner T, Morawetz I, De Col L T, Schneider F, Leitner A, Pressler M, Kazakov G A, Beeks K, Sikorsky T, and Schumm T 2024 *Phys. Rev. Lett.* **132** 182501

[66] Zhang C K, Ooi T, Higgins J S, Doyle J F, von der Wense L, Beeks K, Leitner A, Kazakov G A, Li P, Thirolf P G, Schumm T, and Ye J 2024 *Nature* **3** 63
[67] Qiao Z, Gong C Y, Liao Y K, Wang C L, Chan K K, Zhu S, Kim M, Chen Y C 2021 *Nano Lett.* **22** 1425
[68] Yin X F and Peng C 2020 *Photon. Res.* **8** B25
[69] Shvyd'ko Y, Röhlsberger R, Kocharovskaya O *et al.* 2023 *Nature* **622** 471
[70] Abo-Shaeer J R, Raman C, Vogels J M, and Ketterle W 2001 *Science* **292** 476
[71] Kirschbaum T, Schumm T, and Pálffy A 2024 *Phys. Rev. C* **110** 064326